Indonesian Journal of Pharmacy

VOL 37 (2) 2026: 287–298 | RESEARCH ARTICLE

Development and Optimization of Technetium-99m Radiolabeled Chitosan Nanoparticles for Potential Theranostic Applications in Cancer

Amir Firdaus Abdul Aziz[1,2], Fadzilah Hamzah[2], Muchtaridi Muchtaridi[3] and Amirah Mohd Gazzali[1*]

1. School of Pharmaceutical Sciences, Universiti Sains Malaysia, 11800, Penang, Malaysia
2. Department of Nuclear Medicine, Penang General Hospital, 10990, Penang, Malaysia
3. Department of Pharmaceutical Analysis and Medicinal Chemistry, Faculty of Pharmacy, Universitas Padjadjaran, 45363 Sumedang, Indonesia

Article Info

Submitted: 07-02-2025
Revised: 12-04-2026
Accepted: 16-04-2026

*Corresponding author
Amirah Mohd Gazzali

Email:
amirahmg@usm.my

ABSTRACT

Technetium-99m (^{99m}Tc) is widely used in single-photon emission computed tomography (SPECT) imaging due to its favorable physical properties, including a short half-life (6 hours), optimal gamma emission (140 keV), and generator availability. Radiolabeling nanoparticles with ^{99m}Tc offers a promising strategy to enhance targeted imaging and enable theranostic applications. Chitosan nanoparticles, known for their biocompatibility and biodegradability, represent an attractive platform for such applications. This study aimed to develop and characterize chitosan nanoparticles and evaluate their radiolabeling with ^{99m}Tc. Nanoparticles were prepared via ionotropic gelation, and the effects of chitosan concentration and solution pH on particle size were investigated. Radiolabeling was performed using direct methods with and without a reducing agent (stannous chloride), and the efficiency and stability of radiolabeling were assessed. The optimized nanoparticles exhibited sizes ranging from 81 to 270 nm with a narrow size distribution. Radiolabeling in the presence of stannous chloride achieved efficiencies exceeding 90%, with stability maintained for up to 6 hours. In contrast, labeling without a reducing agent resulted in lower efficiency. Transmission electron microscopy confirmed the preservation of spherical morphology following radiolabeling, with a moderate increase in particle size. In conclusion, ^{99m}Tc-radiolabeled chitosan nanoparticles demonstrated favorable physicochemical properties, high labeling efficiency, and good stability, highlighting their potential as a dual-function theranostic platform for cancer imaging and targeted therapy.

Keywords: chitosan, nanoparticles, ionic gelation, SPECT imaging, technetium-99m

INTRODUCTION

Technetium-99m (^{99m}Tc) is widely used in SPECT imaging due to the appealing physical properties that have made it a suitable radiotracer for nuclear medicine. The 6-hour half-life of technetium-99m refers to its physical half-life, which is the time required for the radionuclide to decay by emitting gamma radiation. This property is ideal for diagnostic imaging as it provides sufficient time for imaging procedures while minimizing radiation exposure to the patient. As a diagnostic agent, ^{99m}Tc can be used to detect disease-specific areas or evaluate treatment efficacy, often in conjugation with targeting moieties to enhance its delivery. Among the commonly used targeting agents is methylene diphosphonate (MDP), which is made available in clinical diagnostic kits. In recent years, there has been an increase in research interest related to the application of chitosan nanoparticles as drug delivery carriers. Numerous methods can be used to produce chitosan nanoparticles, such as emulsification/solvent evaporation, polyelectrolyte complexation, reverse micellar/ microemulsion, and ionotropic gelation. The first reported synthesis of chitosan nanoparticles by

Ohya et al. (1994) used the emulsification and cross-linking method (Ohya et al., 1994; Zhang et al., 2021).

Moreover, nanoparticles are gaining traction as theranostic agents, due to their ability to provide both diagnostic imaging and therapeutic delivery. Their advantages include targeted delivery (He et al., 2025) and the enhanced permeability and retention (EPR) effect (Jeon et al., 2022). In addition, Daems et al. (2021) have also highlighted that nanoparticles can hold multiple radionuclides, allowing for significantly higher radioactivity payloads compared to conventional radiopharmaceutical agents. This characteristic will help to increase the detection limit and the resolution of imaging applications. Although chitosan nanoparticles have been widely explored for drug delivery applications, their radiolabeling with technetium-99m remains relatively underreported. In particular, there is limited understanding of how reducing agents such as stannous chloride influence labeling efficiency and stability. In addition, the effect of the radiolabeling process on key physicochemical properties, including particle size and morphology, has not been extensively investigated. This study aims to develop and characterize chitosan nanoparticles, and the impact of processing parameters on the particle size was examined before the nanoparticles were radiolabeled with ^{99m}Tc. The stability of the radiolabeled complex was further evaluated, and the influence of radiolabeling on the nanoparticle size was investigated using electron microscopy.

MATERIALS AND METHODS

Preparation of Chitosan Nanoparticles

Chitosan nanoparticles were prepared *via* the ionotropic gelation method with some modifications (Sullivan et al., 2018). In this method, chitosan nanoparticles were produced by adding a sodium tripolyphosphate (TPP) 0.05 %w/v solution to a chitosan solution that was stirred at room temperature. Ionic interaction between the positively charged amino functional groups of chitosan and the negatively charged TPP led to the formation of nanoparticles.

Four concentrations of chitosan (0.25, 0.5, 0.75, and 1.0 mg/mL) were prepared in a 100 mL diluted solution of acetic acid (0.15 %v/v) under overnight stirring at 650 rpm at room temperature, followed by 1 hour of sonication at room temperature to complete the solubilization. The pH of the chitosan solution was around 3.4 and was adjusted to the targeted pH (i.e., pH 4.5, 4.6, 4.7, and 5.0) using a 0.1 M NaOH solution.

TPP aqueous solution (0.05% w/v) was then added dropwise into the chitosan solution at room temperature according to the ratio of 3:1 (chitosan to TPP), under magnetic stirring for 45 minutes. The chitosan nanoparticles were then obtained following centrifugation at 4000 rpm for 20 minutes at room temperature (Figure 1).

Characterization of Chitosan Nanoparticles

The hydrodynamic diameter and the size distribution of the chitosan nanoparticles were analyzed by dynamic light scattering in a particle size analyzer (Litesizer 100, Anton Paar). The measurement was done at 25°C with an angle detection of 175°. The surface charge of the particles was also determined using the Malvern Paralytical Zetasizer Nano.

Radiolabeling with ^{99m}Tc

The radiolabeling studies were conducted at the Nuclear Medicine Department, Penang General Hospital. Before the radiolabeling procedure, ^{99m}Tc was eluted from a ^{99}Mo/^{99m}Tc generator and collected in an evacuated vial. In this study, a wet-column generator was used. When handling radioactive materials, the radiation protection principles were followed to minimize radiation exposure. According to Alabsy et al. (2023), the three basic principles of radiation protection are time, distance, and shielding. Radiation exposure has the potential to accumulate with prolonged exposure duration. Minimizing radiation exposure can be achieved through the reduction of exposure time. The principle of maintaining a safe distance is a critical factor to consider in the context of radiation protection. The amount of radiation exposure can be minimized by increasing the distance from the radiation source. Furthermore, the utilization of suitable shielding can effectively minimize the level of radiation exposure.

The purity of the eluted ^{99m}Tc was evaluated through two tests: (1) the molybdenum breakthrough test and (2) the aluminum breakthrough test. The molybdenum breakthrough test was performed using the energy differential method. This involved measuring the eluate in a dose calibrator with the use of a special lead shield, known as the 'moly-shield,' to detect ^{99m}Tc, and without the shield to detect ^{99}Mo, and the expected level of ^{99}Mo presence in the eluate should be below 0.15 µCi per mCi ^{99m}Tc (Ramadhanti & Febriana, 2024).

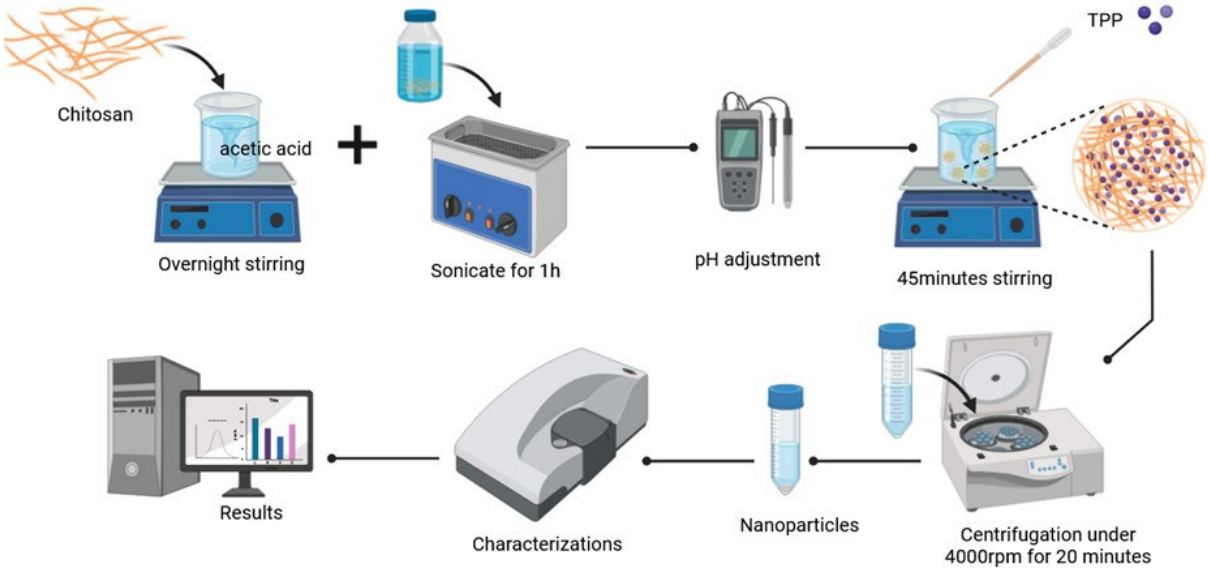

Figure 1. Preparation of chitosan nanoparticles

The aluminum breakthrough test, on the other hand, was carried out by comparing the color intensity of the two spots between the aluminum standard (10µg/mL) and ^{99m}Tc (eluate) (Hasan & Prelas, 2020; Marlina et al., 2022). A drop of standard aluminum solution (10 µg/mL) is placed on one side of the indicator paper, while a drop of ^{99m}Tc eluate is placed on the other. The color intensity of both droplets is then compared. If the ^{99m}Tc drop appears redder than the aluminum standard, the aluminum concentration in the generator eluate exceeds the acceptable limit of 10 µg/mL (Hasan & Prelas, 2020; Marlina et al., 2022).

Then, after ensuring that the obtained ^{99m}Tc passes the test that must be done against the generator eluate, the next step is to radiolabel the chitosan nanoparticles with ^{99m}Tc. The radiolabeling process was conducted through two methods: (1) direct labeling without a reducing agent, and (2) direct labeling in the presence of stannous chloride as a reducing agent (Banerjee et al., 2005; Rajabi et al., 2016). In the first method, a clean, empty vial was filled with 100µL of chitosan nanoparticles solution. Then, to minimize the radiation exposure during the radiolabeling process, the vial containing the nanoparticles is placed inside the lead vial shield. Next, 100-111 MBq (2.7–3.0 mCi) of freshly eluted sodium ^{99m}Tc pertechnetate in 0.5 mL of 0.9% sodium chloride was withdrawn from the evacuated vial using a syringe shield and added to the solution of nanoparticles.

In the second method (Rajabi et al., 2016), a clean, empty vial that was filled with 100µL of chitosan nanoparticles solution was added to it with 0.25µL of freshly prepared stannous chloride (0.2 mg/mL, w/v) in 0.02 N HCl. The vial containing the mixture is placed inside the lead vial shield. Then, 100-111 MBq (2.7–3.0 mCi) of freshly eluted sodium ^{99m}Tc pertechnetate in 0.5 mL of 0.9% sodium chloride was withdrawn from the evacuated vial using a syringe shield and added to the mixture. The solution was then gently swirled for 10 seconds after being filled up to 1 mL with normal saline. The radiolabeled complex was then incubated for 30 minutes at room temperature. The radiochemical purity of the radiolabeled complex was determined using radio-TLC, and a pH meter was used to determine the pH of the complex.

Characterization of ^{99m}Tc-labeled Chitosan Nanoparticles

Labeling Efficiency of ^{99m}Tc-labeled Chitosan Nanoparticles

The labeling efficiency of ^{99m}Tc-labeled chitosan nanoparticles was ascertained through the instant thin-layer chromatography (ITLC) method. In this method, Whatman 31ET (0.7 x 6 cm) paper (Gelman Sciences Inc., Ann Arbor, MI, USA) is used as the stationary phase, and the chromatography was performed using acetone as the mobile phase.

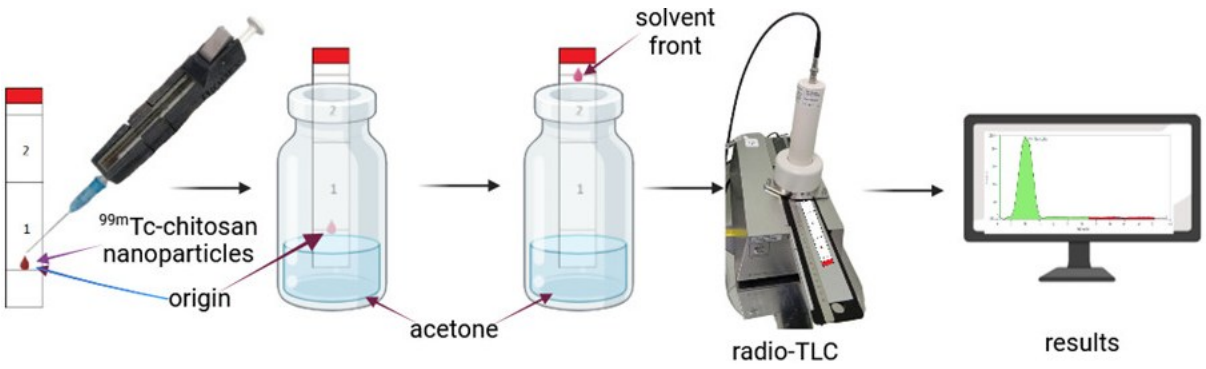

Figure 2. The radiolabeling efficiency test for ^{99m}Tc-labeled chitosan nanoparticles.

Acetone was poured into the vial to a depth of about 5 mm. One drop (approximately 5µL) of the sample (^{99m}Tc-labeled chitosan nanoparticles) was placed on the first line at the bottom of the strip and placed into the developing vial (the origin was ensured to be higher than the solvent) (Figure 2). The solvent was then allowed to rise to the top line (solvent front) of the strip. The contaminants were identified as free ^{99m}Tc pertechnetate (unlabeled ^{99m}Tc). The free ^{99m}Tc pertechnetate, which migrates with the solvent front (rf = 1.0), was estimated in the range of 15–20% of the total radioactivity added (Banerjee et al., 2005). The total labeling of chitosan nanoparticles (^{99m}Tc-labeled chitosan nanoparticles) was determined through analysis of the ITLC by radio-TLC. The data obtained was recorded accordingly. The stability of radiolabeled nanoparticles was monitored at room temperature. To test the stability of ^{99m}Tc-labeled chitosan nanoparticles, the same method as labeling efficiency was used. In this study, the samples were analyzed at various time points: 30, 60, 120, 240, 300, and 360 minutes after preparation. This procedure was repeated with the other ^{99m}Tc-labeled chitosan nanoparticles.

Transmission Electron Microscope Images

Transmission electron microscopy (TEM) (CM12® FEI, Eindhoven, Netherlands) at a voltage of 100 kV was used to investigate the morphology of nanoparticles before and after labeling. The nanoparticle suspension was adequately diluted. A drop was taken using a micropipette and placed on a carbon-coated copper grid. The excess suspension was removed by blotting the grid with filter paper. After that, the deposit was allowed to dry before analysis.

RESULTS AND DISCUSSION

In this study, chitosan nanoparticles were prepared through the ionotropic gelation method. The effect of chitosan concentrations on nanoparticle size was determined by evaluating four concentrations of chitosan: 0.25, 0.5, 0.75, and 1.0 mg/mL. The initial pH of the prepared chitosan solution was also adjusted to evaluate the effect of pH on the particle size of the prepared chitosan nanoparticles.

During the process, chitosan nanoparticles spontaneously develop when ionic cross-linking occurs between the positively charged amino groups on the chitosan chain and the negatively charged TPP, leading to the formation of the nanoparticles. TPP was added to the prepared chitosan solution with a fixed ratio of 3:1 chitosan to TPP. This specific ratio was chosen due to several studies conducted previously showing that the ratio was successful in producing relatively small nanoparticle sizes (Des Bouillons-Gamboa et al., 2024; Hassani et al., 2015; Hejjaji et al., 2018; Masarudin et al., 2015). Based on the observation, immediately after the addition of TPP to the chitosan solution, chitosan with a concentration of 0.25 mg/mL at pH 4.6 failed to form a clear solution. Instead, it produced an opalescent solution. The opalescence observed in the solution after the addition of TPP could probably be attributed to the inadequate crosslinking of chitosan and TPP, resulting in the incomplete formation of nanoparticles (Cho et al., 2014). The formed chitosan nanoparticle suspension was then centrifuged to purify the nanoparticles before the particle size was determined.

Characterization of Chitosan Nanoparticles

Following the preparation of the chitosan nanoparticles, several parameters were analyzed, including particle size, surface charge, and morphological characteristics. Particle size measurement is one of the most important criteria in evaluating the effectiveness of methods used to produce nano-sized particles. Chitosan nanoparticles should be relatively small when initially produced. This is because any modification or encapsulation of drugs within the nanoparticles could increase the particle sizes. The uniformity of particle size distribution in a sample is reflected by the polydispersity index (PDI). Having a high PDI value implies that there is a wide size variation among the nanoparticles present, which may lead to the development of aggregates and, in turn, poor stability and homogeneity of the particle suspension (Nerli et al., 2023). The particle size was analyzed using a particle size analyzer (Anton Paar Litesizer™ 100, Austria), which examined the hydrodynamic diameter as well as the PDI for each nanoparticle sample.

The surface charge of nanoparticles is another important parameter in the characterization of nanoparticles. This surface charge is indicated by the zeta potential, which is related to the degree of repulsion between charged particles in the dispersion. A high zeta potential indicates that the particles are highly charged, and this condition prevents particle aggregation due to electrostatic repulsion, which in turn confers stability (Zhuxin et al., 2023). On the other hand, a low zeta potential implies that the attractive forces may exceed this repulsion, which may promote the particle to coagulate (Athavale et al., 2022; Huang et al., 2022). In the present study, the zeta potential analyzer (Malvern Zetasizer Nano-Z, Malvern Instruments, UK) was used to measure the zeta potential in determining the stability of the nanoparticle suspensions.

Thakur and Taranjit (2011) previously reported that the zeta potential measured for the preparation of chitosan nanoparticles (at pH 5.0) utilizing the ionotropic gelation method ranged from +14.7 mV to +35.5 mV. The study's data indicate a correlation between the measured zeta potential and the concentrations of chitosan and TPP utilized. A zeta potential of +14.7 mV was acquired through the formation of chitosan particles with a size of 635.2 nm using a chitosan concentration of 0.2% w/v and a TPP concentration of 0.086% w/v. Upon decreasing the concentration of TPP to 0.042% w/v while keeping the chitosan concentration constant at 0.2% w/v, an increase in the zeta potential to +17.4 mV and a particle size of 123.5 nm were observed. The result showed the role of TPP in the formation of small particles, but it does not influence the surface charge significantly. In the current formulation, the surface charge is highly determined by the cationic charge of the chitosan polymer, which is evidenced by the significant increase in the zeta potential (+35.5 mV) when the chitosan concentration was increased to 0.56 %w/v. As previously reported in the literature, the preparation of chitosan nanoparticles *via* the ionic gelation method will usually produce nano-sized particles that rarely exceed 250 nm in size (Miladi et al., 2015). However, this rule is still governed by several factors. Hejjaji et al. (2018) evaluated the influence of chitosan on TPP ratios on the size of nanoparticles produced, and were tested at a constant pH (pH 5). The results of the study showed that the 3:1 ratio (chitosan to TPP) gave the smallest particle size. Thus, this exact ratio was used in this study, whilst two other factors were varied: chitosan concentration and medium pH (Figure 3).

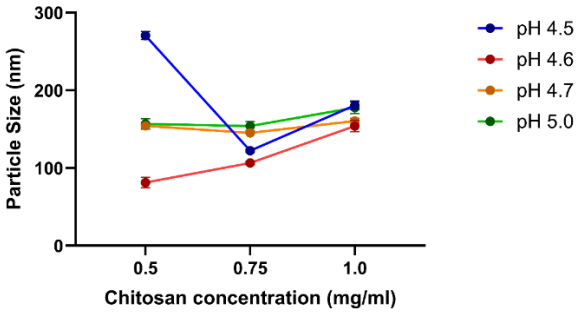

Figure 3. Effect of chitosan concentration (mg/mL) on particle sizes (nm) at four pH conditions; (A) pH 4.5, (B) pH 4.6, (C) pH 4.7, (D) pH 5.0 (n=3)

From the study conducted, certain concentrations are unsuitable for the production of chitosan nanoparticles. For each of the four pHs tested (4.5, 4.6, 4.7, and 5.0), chitosan at a concentration of 0.25 mg/ml failed to yield nano-sized chitosan. This could be due to the presence of a relatively lower number of positively charged amino groups from the chitosan chain at lower chitosan concentration. Hence, the failure of chitosan nanoparticle production might be attributed to an excess anionic charge from TPP in comparison to the cationic charge present in the solution. This outcome is consistent with the

finding reported by Mirtajaddini et al. (2021), in which, at 0.25 mg/mL, the authors have also described the presence of larger-diameter complexes and agglomerates of particles.

At higher chitosan concentrations, nano-sized chitosan nanoparticles were effectively produced with a size ranging between 81 and 270 nm. The increment in chitosan concentration will lead to an increment in the particle size as well (Sreekumar et al., 2018; Zelenková et al., 2018). This pattern is seen at pH 4.6, in which the increment in the chitosan concentration has led to an increment in particle size. However, this is not the pattern observed at the other pH conditions. In pH 4.7 and pH 5.0, there was a reduction in particle size at 0.75 mg/mL, followed by an increment at 1 mg/mL, whilst at pH 4.5, the particle size reduced from 0.5 mg/mL to 1 mg/mL, with the smallest particle size recorded at 0.75 mg/mL. Hence, using chitosan solution at pH 4.6 may provide a more predictable pattern of particle size changes as compared to the other tested pH conditions. The observed correlation between the concentration of chitosan and the size of the resulting nanoparticles was crucial as it has the potential to influence both the efficacy and stability of the particles being studied. Comprehending this particular pattern may aid researchers in optimizing the concentration of chitosan to attain the intended particle size for specific applications. (Rizvi & Saleh, 2018). A significant effect of chitosan concentration and pH on particle size was observed (two-way ANOVA, $p < 0.0001$).

This finding is consistent with the previously reported data; lower chitosan concentrations resulted in smaller particle sizes and *vice versa*. According to earlier studies, the viscosity of chitosan solution is likewise considerably low at lower chitosan concentrations (Omar Zaki et al., 2015). The solubility of chitosan increases in an environment with lower viscosity. This enhanced solubility facilitates the gelation process and promotes the formation of smaller chitosan nanoparticles (Omar Zaki et al., 2015).

The PDI for all nanoparticle concentrations was less than 0.3 (data not shown). This value indicates that the chitosan nanoparticles produced were homogeneous. Lima et al. (2021) reported a low PDI (<0.3) value of chitosan nanoparticles prepared through the ionotropic gelation method. As PDI is associated with the distribution of nanoparticles, a homogenous nanoparticle suspension will have a PDI value closer to 0, while any value exceeding 0.5 indicates that the nanoparticles produced were heterogeneous (Rosyada et al., 2019).

Effect of Initial pH Value on the Particle Sizes

In general, pH influences the solubility of chitosan in a medium. As chitosan has a pKa of 6.5 (Gutiérrez-Ruíz et al., 2024), the polymeric chain is insoluble at higher pH, but in acidic media at lower pH, the amino group ($-NH_2$) on the chitosan chain will be protonated, inducing solubilization (Blockx et al., 2018). Since chitosan forms a positively charged polyelectrolyte when the amino group is protonated at an acidic pH, this condition will affect both the formation of chitosan nanoparticles and the particle size (Antoniou et al., 2015). This is because the formation of chitosan nanoparticles is related to the cross-linking between the polycation chitosan and the polyanion TPP (chitosan-TPP) (Ruiz-Pulido et al., 2022).

As described by previous studies, pH was found to influence the size of chitosan nanoparticles Mattu et al., 2013). In the present work, the same trend was observed as that reported by Hu et al. (2008); at relatively low pH, the size of the resulting chitosan particles is larger than the size of particles produced in higher pH media. At pH 4.5, the particle size is higher compared to the particle size at pH 4.6 in all concentrations of chitosan examined (0.5, 0.75, and 1.0 mg/mL). The particle size was reduced at pH 4.6 but showed an increasing trend with further increments in pH value for each chitosan concentration examined (0.5, 0.75, and 1.0 mg/ml). These findings are consistent with earlier research, whereby Mattu et al. (2013) showed that the particle size and PDI of chitosan nanoparticles were increased with the increment in the pH of the chitosan solution used, from pH 3.0 (119.8 ±2.6 nm) to pH 5.5 (453.9 ±17.0 nm) with a chitosan/TPP mass ratio 25% w/w. The observed condition could be attributed to the deprotonation of the amino group present on the chitosan chain, which is likely to occur at elevated pH levels. This deprotonation event is known to result in a reduction in solubility and an increase in nanoparticle aggregation (de Moura et al., 2008). Another possibility is that the deprotonation of the amino group may result in a reduction or elimination of electrostatic repulsion among molecules, thereby potentially facilitating particle aggregation (Ribeiro et al., 2020).

Radiolabeling with ^{99m}Tc

The radiolabeling experiments with technetium-99m (^{99m}Tc) were conducted in the Nuclear Medicine Department, Penang General Hospital. The selected nanoparticle formulation was 0.5 mg/mL chitosan concentration at pH 4.6, which produces the smallest particle size and good particle homogeneity with sufficient stability. The nanoparticles were labeled with the radioactive substance, ^{99m}Tc, that was freshly eluted from a ^{99}Mo/^{99m}Tc generator (Ultra-TechneKow FM, Curium, Netherlands).

Before the radiolabeling process was conducted, the ^{99m}Tc obtained from the generator was first tested for purity. It was found that the ^{99m}Tc passed both tests: the molybdenum breakthrough test and the aluminum breakthrough test. The content of ^{99}Mo was 0.007 µCi per mCi of ^{99m}Tc which is within the acceptable limit (<0.15 µCi per mCi ^{99m}Tc) (Ramadhanti & Febriana, 2024). The aluminum breakthrough test, on the other hand, showed that the intensity of the color for the eluate (^{99m}Tc) was lower than that of the standard aluminum solution, suggesting that the eluate contained less than 10 µg/mL of aluminum (Hasan & Prelas, 2020).

After ensuring that the eluate was of high quality, chitosan nanoparticles were radiolabeled with $^{99m}TcO_4^-$ (pertechnetate), which is the chemically stable form of ^{99m}Tc in aqueous media. The labeling was performed through two methods: (1) direct labeling without a reducing agent, and (2) direct labeling in the presence of stannous chloride as a reducing agent.

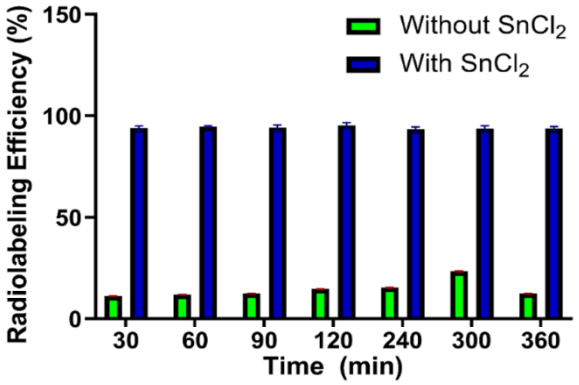

Figure 4 Comparison of radiolabeling efficiency of ^{99m}Tc-labeled chitosan nanoparticle in the absence and presence of SnCl2 over time (n=3)

In Method (1), due to the stability of pertechnetate, the highest labeling efficiency (%) of chitosan nanoparticles recorded was 23.4% at 300 minutes (Figure 4). This is due to the absence of a reducing agent; the pertechnetate remained at a high oxidation state, hence demonstrating a lower labeling efficiency.

In Method (2), the presence of stannous chloride ($SnCl_2$) facilitates the reduction of pertechnetate from its oxidation state +7 to a potentially more reactive form; the +5, +3, or +1 oxidation state (Costa et al., 2019). This reduction enabled the formation of a complex between the pertechnetate and chitosan nanoparticles (Amin et al., 2009; Costa et al., 2019; Zia et al., 2022). More than 90% of the chitosan nanoparticles were radiolabeled with ^{99m}Tc in the presence of $SnCl_2$, as early as 30 minutes after the procedure began, and the radiolabeling efficiency (%) remained at higher than 90% for up to 360 minutes, indicating that the ^{99m}Tc-labeled chitosan nanoparticles have prolonged radiolabeling stability (Kamal et al., 2018). Two-way ANOVA showed that labeling efficiency was significantly higher in the presence of $SnCl_2$ compared to its absence ($p < 0.0001$), with a significant interaction between time and the presence of $SnCl_2$ ($p < 0.0001$). This showed a highly efficient radiolabeling process, on par with the commercially available radiopharmaceutical kit (Banerjee et al., 2005; Gundogdu et al., 2015). Ascorbic acid and ferrous iron have been reported as among the reducing agents of choice for this application. However, both reducing agents are unable to control the reduction reaction, which in turn results in an incomplete reduction process (Costa et al., 2019). Hence, $SnCl_2$ has been used as a reducing agent in many studies (Banerjee et al., 2005; Zia et al., 2022) as it has better control over the overall process, and hence it is now commercially available for radiopharmaceutical use in clinical practice (Mushtaq et al., 2008).

The stability of a radiolabeled product is important, especially in the diagnostic imaging aspect. This is because the instability of this radiolabeled product may cause the quality of the resulting diagnostic image to be poor as a result of the undesired distribution of radioactivity. This situation will further complicate the diagnostic process, as low-quality images would jeopardize the diagnosis process. This is because the unbound ^{99m}Tc released due to the inherent instability of the radiolabeled product may be taken up into non-targeted areas (e.g., thyroid gland, salivary gland, and gastric mucosa) and potentially lead to an error in disease diagnosis (Elgebaly et al., 2023; Miftari et al., 2023).

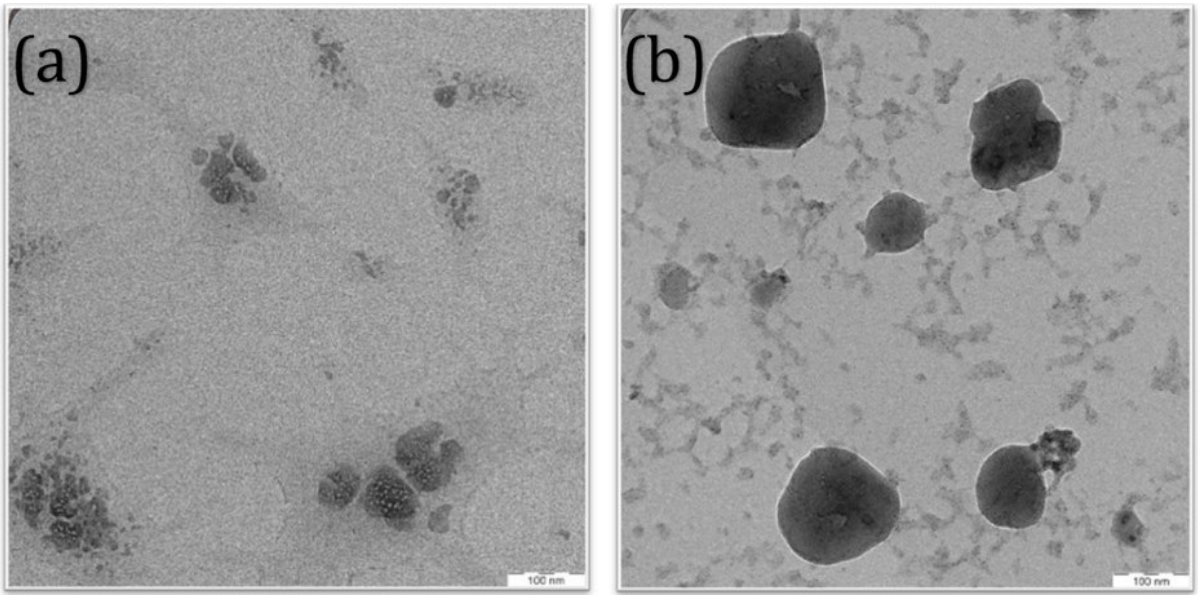

Figure 5. TEM image of unlabelled and ^{99m}Tc radiolabeled chitosan nanoparticles

TEM Images

The unlabelled nanoparticles exhibited an average estimated diameter of 87 nm, which is similar to the size measured using the DLS technique (Figure 5(a)). After the radiolabeling process, the nanoparticle's size increases to an average diameter of 125 nm (Figure 5(b)).

The increase in diameter post-labeling is indicative of the physical incorporation of the radionuclide onto the nanoparticle matrix, a common outcome when particles are modified with radiolabels or other surface modifications. The TEM images also reveal that the morphology of the nanoparticles remains largely spherical after radiolabeling, implying that the structural integrity of the nanoparticles was preserved during the radiolabeling process.

These findings confirm the successful radiolabeling of the chitosan nanoparticles with ^{99m}Tc, which is essential for their potential application in diagnostic imaging or treatment. Furthermore, the consistency between the TEM and DLS measurements highlights the precision of the nanoparticle size estimation techniques used in this study. The size increase due to radiolabeling may also influence the biological interactions of these nanoparticles, particularly their biodistribution, cellular uptake, and clearance, which will need to be further investigated in future studies.

CONCLUSION

Chitosan nanoparticles demonstrated successful radiolabeling with ^{99m}Tc *via* direct labeling in the presence of $SnCl_2$ as the reducing agent. The labeling efficiency (%) exceeded 90%, and the ^{99m}Tc-labeled chitosan nanoparticles maintained their stability for up to 360 minutes. An animal biodistribution study is planned to assess the biodistribution and uptake of the ^{99m}Tc-labeled chitosan nanoparticles. This investigation will provide critical insights into the potential of the nanoparticles as a SPECT imaging agent for diagnosing various diseases, particularly tumors. Furthermore, the study may pave the way for the development of dual-function theranostic agents, offering both diagnostic imaging capabilities and potential applications in targeted drug delivery for therapeutic purposes.

ACKNOWLEDGMENTS

Special thanks to Universiti Sains Malaysia for the Internationalisation Incentive Scheme Grant 2024 (R502-KR-ARP004-00AUPRM003-K134).

CONFLICT OF INTEREST

The authors declare no conflict of interest.

REFERENCES

Alabsy, M. T., Gouda, M. M., Abbas, M. I., Al-Balawi, S. M., & El-Khatib, A. M. (2023). Enhancing the Gamma-Radiation-Shielding Properties

of Gypsum–Lime–Waste Marble Mortars by Incorporating Micro- and Nano-PbO Particles. *Materials*, *16*(4). https://doi.org/10.3390/ma16041577

Amin, M., Jaafari, M. R., & Tafaghodi, M. (2009). Impact of chitosan coating of anionic liposomes on clearance rate, mucosal and systemic immune responses following nasal administration in rabbits. *Colloids and Surfaces B: Biointerfaces*, *74*(1), 225–229. https://doi.org/10.1016/j.colsurfb.2009.07.024

Antoniou, J., Liu, F., Majeed, H., Qi, J., Yokoyama, W., & Zhong, F. (2015). Physicochemical and morphological properties of size-controlled chitosan-tripolyphosphate nanoparticles. *Colloids and Surfaces A: Physicochemical and Engineering Aspects*, *465*, 137–146. https://doi.org/10.1016/j.colsurfa.2014.10.040

Athavale, R., Sapre, N., Rale, V., Tongaonkar, S., Manna, G., Kulkarni, A., & Shirolkar, M. M. (2022). Tuning the surface charge properties of chitosan nanoparticles. *Materials Letters*, *308*. https://doi.org/10.1016/j.matlet.2021.131114

Banerjee, T., Singh, A. K., Sharma, R. K., & Maitra, A. N. (2005). Labeling efficiency and biodistribution of Technetium-99m labeled nanoparticles: Interference by colloidal tin oxide particles. *International Journal of Pharmaceutics*, *289*(1–2), 189–195. https://doi.org/10.1016/j.ijpharm.2004.09.022

Blockx, J., Verfaillie, A., Thielemans, W., & Muylaert, K. (2018). Unravelling the Mechanism of Chitosan-Driven Flocculation of Microalgae in Seawater as a Function of pH. *ACS Sustainable Chemistry and Engineering*, *6*(9), 11273–11279. https://doi.org/10.1021/acssuschemeng.7b04802

Cho, A. R., Chun, Y. G., Kim, B. K., & Park, D. J. (2014). Preparation of Chitosan-TPP Microspheres as Resveratrol Carriers. *Journal of Food Science*, *79*(4). https://doi.org/10.1111/1750-3841.12395

Costa, B., Ilem-Özdemir, D., & Santos-Oliveira, R. (2019). Technetium-99m metastable radiochemistry for pharmaceutical applications: old chemistry for new products. In *Journal of Coordination Chemistry* (Vol. 72, Issue 11, pp. 1759–1784). Taylor and Francis Ltd. https://doi.org/10.1080/00958972.2019.1632838

Daems, N., Michiels, C., Lucas, S., Baatout, S., & Aerts, A. (2021). Gold nanoparticles meet medical radionuclides. In *Nuclear Medicine and Biology* (Vols. 100–101, pp. 61–90). Elsevier Inc. https://doi.org/10.1016/j.nucmedbio.2021.06.001

de Moura, M. R., Aouada, F. A., & Mattoso, L. H. C. (2008). Preparation of chitosan nanoparticles using methacrylic acid. *Journal of Colloid and Interface Science*, *321*(2), 477–483. https://doi.org/10.1016/j.jcis.2008.02.006

Des Bouillons-Gamboa, R. E., Montes de Oca, G., Baudrit, J. R. V., Ríos Duarte, L. C., Lopretti, M., Rentería Urquiza, M., Zúñiga-Umaña, J. M., Barreiro, F., & Vázquez, P. (2024). Synthesis of chitosan nanoparticles (CSNP): effect of CH-CH-TPP ratio on size and stability of NPs. *Frontiers in Chemistry*, *12*. https://doi.org/10.3389/fchem.2024.1469271

Elgebaly, R. H., Rageh, M. M., Adel, M., & Kamal, I. (2023). Studying Various Parameters Affecting Labeling Efficiency Of Radiopharmaceuticals In Nuclear Medicine. *Journal of Pharmaceutical Negative Results ¦*, *14*(02), 3512–3520. https://doi.org/10.47750/pnr.2023.14.02.413

Gundogdu, E., Ilem-Ozdemir, D., Ekinci, M., Ozgenc, E., & Asikoglu, M. (2015). Radiolabeling efficiency and cell incorporation of chitosan nanoparticles. *Journal of Drug Delivery Science and Technology*, *29*, 84–89. https://doi.org/10.1016/j.jddst.2015.06.018

Gutiérrez-Ruíz, S. C., Cortes, H., González-Torres, M., Almarhoon, Z. M., Gürer, E. S., Sharifi-Rad, J., & Leyva-Gómez, G. (2024). Optimize the parameters for the synthesis by the ionic gelation technique, purification, and freeze-drying of chitosan-sodium tripolyphosphate nanoparticles for biomedical purposes. *Journal of Biological Engineering*, *18*(1). https://doi.org/10.1186/s13036-024-00403-w

Hasan, S., & Prelas, M. A. (2020). Molybdenum-99 production pathways and the sorbents for 99Mo/99mTc generator systems using (n, γ) 99Mo: a review. *SN Applied Sciences*, *2*(11),

1–28. https://doi.org/10.1007/s42452-020-03524-1

Hassani, S., Laouini, A., Fessi, H., & Charcosset, C. (2015). Preparation of chitosan-TPP nanoparticles using microengineered membranes - Effect of parameters and encapsulation of tacrine. *Colloids and Surfaces A: Physicochemical and Engineering Aspects*, *482*, 34–43. https://doi.org/10.1016/j.colsurfa.2015.04.006

He, J., Yang, L., Li, D., Xie, J., Zhou, G., Zhou, R., Li, Y., Wei, G., Gong, Z., Li, L., Lai, K., & Zhou, J. (2025). Transferrin-modified carboxymethyl chitosan-chitosan nanoparticles as an efficient delivery carrier for targeted therapy of depression. *International Journal of Biological Macromolecules*, *286*. https://doi.org/10.1016/j.ijbiomac.2024.138352

Hejjaji, E. M. A., Smith, A. M., & Morris, G. A. (2018). Evaluation of the mucoadhesive properties of chitosan nanoparticles prepared using different chitosan to tripolyphosphate (CS:TPP) ratios. *International Journal of Biological Macromolecules*, *120*, 1610–1617. https://doi.org/10.1016/j.ijbiomac.2018.09.185

Huang, M., Xu, Y., Xu, L., Bai, Y., & Xu, X. (2022). Interactions of water-soluble myofibrillar protein with chitosan: Phase behavior, microstructure and rheological properties. *Innovative Food Science and Emerging Technologies*, *78*. https://doi.org/10.1016/j.ifset.2022.103013

Jeon, S., Jun, E., Chang, H., Yhee, J. Y., Koh, E. Y., Kim, Y., Jung, J. Y., Jeong, E. J., Lee, J. W., Shim, M. K., Yoon, H. Y., Chang, S., Kim, K., & Kim, S. C. (2022). Prediction the clinical EPR effect of nanoparticles in patient-derived xenograft models. *Journal of Controlled Release*, *351*, 37–49. https://doi.org/10.1016/j.jconrel.2022.09.007

Kamal, R., Chadha, V. D., & Dhawan, D. K. (2018). Physiological uptake and retention of radiolabeled resveratrol loaded gold nanoparticles (99mTc-Res-AuNP) in colon cancer tissue. *Nanomedicine: Nanotechnology, Biology, and Medicine*, *14*(3), 1059–1071. https://doi.org/10.1016/j.nano.2018.01.008

Lima, K. O., Pinilla, C. M. B., Alemán, A., López-Caballero, M. E., Gómez-Guillén, M. C., Montero, P., & Prentice, C. (2021). Characterization, bioactivity and application of chitosan-based nanoparticles in a food emulsion model. *Polymers*, *13*(19). https://doi.org/10.3390/polym13193331

Marlina, Sarmini, E., Lestari, E., Pratama, C., Nurmanjaya, A., Sriyono, Abidin, Triyatna, F., Kadarisman, Aries, A., Febriana, S., Setiawan, H., Saptiama, I., Mujamilah, Patriati, A., Awaludin, R., & Yulizar, Y. (2022). Surface modification of acid-functionalized mesoporous gamma-alumina for non-fission 99Mo/99mTc generator. *Applied Radiation and Isotopes*, *187*. https://doi.org/10.1016/j.apradiso.2022.110342

Masarudin, M. J., Cutts, S. M., Evison, B. J., Phillips, D. R., & Pigram, P. J. (2015). Factors determining the stability, size distribution, and cellular accumulation of small, monodisperse chitosan nanoparticles as candidate vectors for anticancer drug delivery: Application to the passive encapsulation of [14C]-doxorubicin. *Nanotechnology, Science and Applications*, *8*, 67–80. https://doi.org/10.2147/NSA.S91785

Mattu, C., Li, R., & Ciardelli, G. (2013). Chitosan nanoparticles as therapeutic protein nanocarriers: The effect of ph on particle formation and encapsulation efficiency. *Polymer Composites*, *34*(9), 1538–1545. https://doi.org/10.1002/pc.22415

Miftari, R., Maloku, H., Bajqinca, A., Rexhaj, B., Miftari, S., Kaqiu, Y., & Mansoob Khan, M. (2023). The Role of Dynamic (99m) Tc Pertechnetate Scintigraphy in Early Detection and Differentiation of Hyperthyroidism. *Journal of Medicinal and Chemical Sciences*, *6*(9), 2177–2185. https://doi.org/10.26655/JMCHEMSCI.2023.9.23

Miladi, K., Sfar, S., Fessi, H., & Elaissari, A. (2015). Enhancement of alendronate encapsulation in chitosan nanoparticles. *Journal of Drug Delivery Science and Technology*, *30*, 391–396. https://doi.org/10.1016/j.jddst.2015.04.007

Mirtajaddini, S. A., Najafi, M. F., Yazdi, S. A. V., & Oskuee, R. K. (2021). Preparation of Chitosan Nanoparticles as a Capable Carrier for Antigen Delivery and Antibody Production. *Iranian Journal of Biotechnology*, *19*(4), 32–40. https://doi.org/10.30498/ijb.2021.247747.2871

Mushtaq, A., Rehman, T. U., Mansur, M. S., & Jehangir, M. (2008). Adsorption of99mTc-radiopharmaceuticals onto injection vials and syringes. *Journal of Nuclear Medicine Technology*, *36*(2), 91–94. https://doi.org/10.2967/jnmt.107.048561

Nerli, G., Gonçalves, L. M. D., Cirri, M., Almeida, A. J., Maestrelli, F., Mennini, N., & Mura, P. A. (2023). Design, Evaluation and Comparison of Nanostructured Lipid Carriers and Chitosan Nanoparticles as Carriers of Poorly Soluble Drugs to Develop Oral Liquid Formulations Suitable for Pediatric Use. *Pharmaceutics*, *15*(4). https://doi.org/10.3390/pharmaceutics15041305

Ohya, Y., Shiratani, M., Kobayashi, H., & Ouchi, T. (1994). Release behavior of 5-fluorouracil from chitosan-gel nanospheres immobilizing 5-fluorouracil coated with polysaccharides and their cell specific cytotoxicity. *Journal of Macromolecular Science, Part A*, *31*(5), 629–642. https://doi.org/10.1080/10601329409349743

Rajabi, H., Rasaneh, S., & Salehi, S. (2016). Synthesis and Biological Evaluation of 99mTc-Chitosan Nanoparticles as a Potential Radiopharmaceutical for Liver Imaging. *Synthesis and Reactivity in Inorganic, Metal-Organic and Nano-Metal Chemistry*, *46*(10), 1450–1454. https://doi.org/10.1080/15533174.2015.1137010

Ramadhanti, N. Z., & Febriana, S. (2024). Verification on Molybdenum-99 (99Mo) Breakthrough from Non-Fission 99Mo/99mTc Generator to Produce Technetium-99m (99mTc) Medical Radionuclide. *Journal of Physics: Conference Series*, *2866*(1). https://doi.org/10.1088/1742-6596/2866/1/012056

Ribeiro, E. F., de Barros-Alexandrino, T. T., Assis, O. B. G., Junior, A. C., Quiles, A., Hernando, I., & Nicoletti, V. R. (2020). Chitosan and crosslinked chitosan nanoparticles: Synthesis, characterization and their role as Pickering emulsifiers. *Carbohydrate Polymers*, *250*. https://doi.org/10.1016/j.carbpol.2020.116878

Rizvi, S. A. A., & Saleh, A. M. (2018). Applications of nanoparticle systems in drug delivery technology. In *Saudi Pharmaceutical Journal* (Vol. 26, Issue 1, pp. 64–70). Elsevier B.V. https://doi.org/10.1016/j.jsps.2017.10.012

Rosyada, A., Sunarharum, W. B., & Waziiroh, E. (2019). Characterization of chitosan nanoparticles as an edible coating material. *IOP Conference Series: Earth and Environmental Science*, *230*(1). https://doi.org/10.1088/1755-1315/230/1/012043

Ruiz-Pulido, G., Quintanar-Guerrero, D., Serrano-Mora, L. E., & Medina, D. I. (2022). Triborheological Analysis of Reconstituted Gastrointestinal Mucus/Chitosan:TPP Nanoparticles System to Study Mucoadhesion Phenomenon under Different pH Conditions. *Polymers*, *14*(22). https://doi.org/10.3390/polym14224978

Sreekumar, S., Goycoolea, F. M., Moerschbacher, B. M., & Rivera-Rodriguez, G. R. (2018). Parameters influencing the size of chitosan-TPP nano- and microparticles. *Scientific Reports*, *8*(1). https://doi.org/10.1038/s41598-018-23064-4

Sullivan, D. J., Cruz-Romero, M., Collins, T., Cummins, E., Kerry, J. P., & Morris, M. A. (2018). Synthesis of monodisperse chitosan nanoparticles. *Food Hydrocolloids*, *83*, 355–364. https://doi.org/10.1016/j.foodhyd.2018.05.010

Thakur, A., & Taranjit. (2011). Preparation of chitosan nanoparticles: A study of influencing factors. *AIP Conference Proceedings*, *1393*, 299–300. https://doi.org/10.1063/1.3653728

Zaki O, Sarah S., Ibrahim, M. N., & Katas, H. (2015). Particle size affects concentration-dependent cytotoxicity of chitosan nanoparticles towards mouse hematopoietic stem cells. *Journal of Nanotechnology*, *2015*. https://doi.org/10.1155/2015/919658

Zelenková, T., Mora, M. J., Barresi, A. A., Granero, G. E., & Fissore, D. (2018). On the Production of Chitosan-Coated Polycaprolactone

Nanoparticles in a Confined Impinging Jet Reactor. *Journal of Pharmaceutical Sciences*, *107*(4), 1157–1166. https://doi.org/10.1016/j.xphs.2017.11.020

Zhang, K., Xu, Y., Lu, L., Shi, C., Huang, Y., Mao, Z., Duan, C., Ren, X., Guo, Y., & Huang, C. (2021). Hydrodynamic cavitation: A feasible approach to intensify the emulsion cross-linking process for chitosan nanoparticle synthesis. *Ultrasonics Sonochemistry*, *74*. https://doi.org/10.1016/j.ultsonch.2021.105551

Zhuxin, L., Biao, Y., Badamkhand, D., Yifan, C., Honghong, S., Xiao, X., Mingqian, T., Zhixiang, W., & Chongjiang, C. (2023). Carboxylated chitosan improved the stability of phycocyanin under acidified conditions. *International Journal of Biological Macromolecules*, *233*. https://doi.org/10.1016/j.ijbiomac.2023.123474

Zia, N., Iqbal, Z., Raza, A., Zia, A., Shafique, R., Andleeb, S., & Walker, G. C. (2022). Glycol-Chitosan-Based Technetium-99m-Loaded Multifunctional Nanomicelles: Synthesis, Evaluation, and In Vivo Biodistribution. *Nanomaterials*, *12*(13). https://doi.org/10.3390/nano12132198